Thin-Films on Cellulose Paper to Construct Thermoelectric Generator of Promising Power Outputs Suitable for Low-Grade Heat Recovery

Rafiq Mulla, Daniel R. Jones, Charles W. Dunnill

PII: S2352-4928(21)00729-7

DOI: https://doi.org/10.1016/j.mtcomm.2021.102738

Reference: MTCOMM102738

To appear in: *Materials Today Communications*

Received date: 15 June 2021
Revised date: 20 August 2021
Accepted date: 20 August 2021

Please cite this article as: Rafiq Mulla, Daniel R. Jones and Charles W. Dunnill, Thin-Films on Cellulose Paper to Construct Thermoelectric Generator of Promising Power Outputs Suitable for Low-Grade Heat Recovery, *Materials Today Communications,* (2021) doi:https://doi.org/10.1016/j.mtcomm.2021.102738

Thin-Films on Cellulose Paper to Construct Thermoelectric Generator of Promising Power Outputs Suitable for Low-Grade Heat Recovery

Rafiq Mulla, Daniel R. Jones and Charles W. Dunnill*

Energy Safety Research Institute, Swansea University, Bay Campus, Fabian Way, Swansea, SA1 8EN, UK.

E-mail address: c.dunnill@swansea.ac.uk

Abstract: Here, cellulose paper-based thermoelectric generators packaged inside Kapton layers are fabricated that demonstrate enhanced physical stability and flexibility with impressive power outputs at low temperature heating. The work introduces a successful combination of copper iodide (CuI) and bismuth (Bi) coated cellulose papers, two non-toxic and simple conductors which act as p-type and n-type legs in the generator, respectively. The power output characteristics of a generator comprising ten p-n junctions are measured and analysed at different temperature gradients. A high output voltage of 84.5 mV and corresponding output power of 215 nW are obtained from the device at a temperature difference (ΔT) of ~50 ºC, which is comparable to expensive and toxic thermoelectric devices reported in the literature. The presented device fabrication method is a very simple and economical approach to fabricate paper based eco-friendly thermoelectric devices that can be used for low-grade heat conversion applications.

Keywords: Thermoelectric; CuI; paper generator; bismuth; device fabrication

Introduction

About two-thirds of all the energy produced on this planet is irreversibly dissipated as waste heat [1, 2]. Thermoelectric materials directly convert temperature gradients into electrical power and can play an important role in future energy needs [3]. Thermoelectric generators have the potential to be applied in waste heat recovery systems and can also be used to generate “clean fuel” hydrogen by supplying electricity to the water electrolysis units from waste heat [4-8]. Conversion of waste heat into electric power offers alternative energy that can help reduce our dependence on fossil fuels. Recent years have witnessed significant interests in thermoelectric research in order to scavenge waste heat by thermoelectric generators [9-15].

Thermoelectric devices work according to the principle of the Seebeck effect to generate electric power from temperature difference; for this reason, maintaining a high temperature gradient across the device is essential to generate a practically useful voltage output. It follows trivially that the voltage produced by a thermoelectric generator may be enhanced by employing thin films of suitable leg length which can hold higher temperature differences as compared to their bulk counterparts [16]. Also, it is useful to minimise device size/thickness [17], and, by limiting system weight, thin-film configurations also afford greater specific power density than their bulk (3D) counterparts with respect to thermoelectric material consumption [18]. Furthermore, thin-films enable the development of versatile systems suited to an array of applications, such as wearable devices prepared using flexible substrates [19-21]. Relative to 3D designs, additional advantages of thin-film-based devices include the reduced consumption of raw materials, rapid fabrication, and waste minimisation. Currently, however, thermoelectric devices are typically prepared using expensive and toxic materials in conjunction with difficult and energy-intensive manufacturing procedures [22-25].

Here, a simple cellulose paper-based fabrication protocol is presented that utilises cost-effective and low-toxicity thermoelectric materials, with the resulting generators exhibiting promising power outputs at low temperatures. The devices consisted of copper iodide (CuI) and bismuth (Bi) films deposited as p- and n-type legs, respectively, on cellulose paper substrates. In addition to exhibiting high p-type conductivity, CuI also possesses extremely low thermal conductivity (0.5 W m^{-1} K^{-1})[26] and a characteristically high Seebeck coefficient [26-28], making it an attractive semiconductor for thermoelectric applications [26, 29], Similarly, Bi was selected due to its n-type semi-metallic behaviour, with the material displaying a higher Seebeck coefficient and lower thermal conductivity than most other metals [30-32]. By utilising cellulose paper as a substrate for the configuration, it was ensured that the devices were economical and able to sustain a high temperature gradient; notably, the thermal conductivity of cellulose paper (0.07-0.10 W m^{-1} K^{-1}) [33] is lower than the corresponding values for CuI, Bi and borosilicate glass (1.0-2.0 W m^{-1} K^{-1}) [34, 35], with the latter used as a common substrate material in thermoelectric generators reported throughout the literature [11, 26]. The abundance and degradable nature of cellulose paper can assist in the fabrication of cheap and disposable electronic devices [36, 37]. However, fibrous surface of cellulose paper can have adverse effects on electrical conductivity if the deposited films are extremely thin. Therefore, thin films with sufficient thickness have been used to minimize such effects on conductivity. In order to further enhance devices stability and flexibility, a Kapton tape (polyimide) was selected as the base of the device for being flexible and robust, including its advantages such as low thermal conductivity (0.12 W m^{-1} K^{-1}) and thermal stability at high working temperatures [38].

Experimental Details

Thin film deposition

Copper (99.7% purity) and bismuth (99.9% purity) sputter targets, used as primary sources to deposit respective thin films, were obtained from Kurt J. Lesker Company Ltd. and PI-KEM Ltd., respectively. Cu and Bi films (thickness: 200 nm, deposition rate: ~20 nm min^{-1}) were deposited by sputter-coating (Model: Quorum Q150T S coater) onto cellulose paper substrates (size: 8 cm x 3 cm, paper thickness: 100 µm) at room temperature under argon atmosphere. The sputtering chamber was evacuated to 10^{-4} mbar prior to each deposition run.

Conversion of Cu film into CuI film

CuI thin-films on cellulose paper were obtained by the reaction of sputtered Cu thin-films with iodine vapour. In a closed petri dish (diameter: 15 cm, height: 1.5 cm), solid iodine granules (1 g, Sigma-Aldrich) were evenly spread beneath the Cu-sputtered paper, which was mounted horizontally at a distance of 1.5 cm above the iodine granules with the Cu thin-film facing downwards (supported by a adhesive tape at the paper borders); this iodination setup is illustrated schematically in Figure 1. The formation of CuI from reaction of iodine vapour ($I_{2(g)}$) with metal copper ($Cu_{(s)}$) can be expressed as [27]:

$$2Cu_{(s)} + I_{2(g)} \rightarrow 2CuI \quad \text{..... (1)}$$

Complete conversion of the Cu film to CuI was achieved after 5 h of reaction at 40 ºC, with heating provided by a hot-plate.

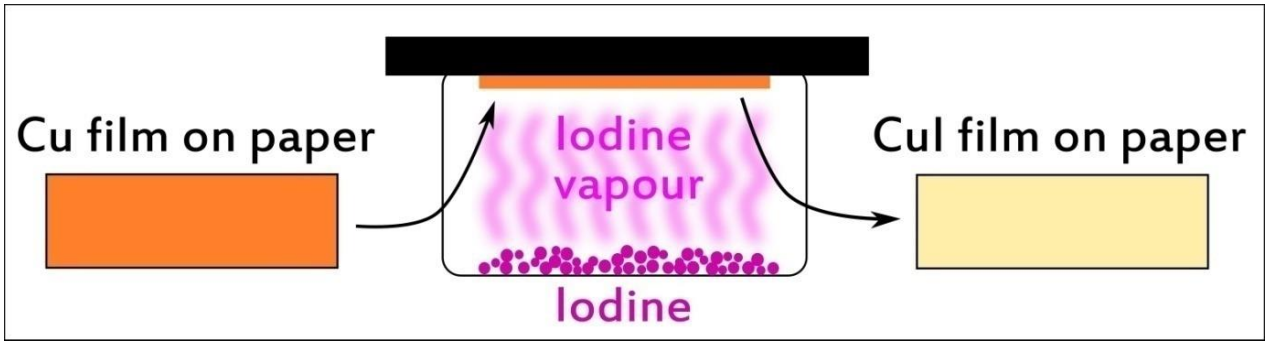

Figure 1. Schematic illustration of the configuration employed to prepare CuI thin-films on cellulose paper through reaction of sputtered Cu thin-films with iodine vapour.

Fabrication of paper based thermoelectric generators

The as-obtained CuI- and Bi-sputtered cellulose paper substrates were cut into strips (length: 10 mm or 20 mm, width: 5 mm) to act as p- and n-type legs, respectively, of two planar ten pair thermoelectric devices (L10 and L20 with leg lengths 10 mm and 20 mm, respectively); all of the steps involved in the preparation of these CuI- and Bi-sputtered strips are illustrated in Figure 2. Each of the thermoelectric devices comprised ten pairs of alternating p-type (CuI) and n-type (Bi) paper strips connected in a series configuration using copper foil and carbon conductive paint, with high-temperature polyimide tape placed beneath the strips to secure them in position (Note: the effective leg lengths of the device L10 and L20 after connecting with copper foils were ~6 mm and ~16 mm, respectively). After complete drying of conductive paint of each as-constructed device at 50 ºC (on a hot-plate for 2 hr), its upper surface was also covered with polyimide tape, which was then pressed using a press machine (model: Devilpress, Swizzex Group Ltd.) under 10 MPa pressure (at room temperature for 1 min) in order to increase the structural stability of the system and to avoid exposure of the CuI and Bi films to air. Sequential photographs of the assembly process are shown in Figure 3. In order to compare the output properties, single pair devices of leg length 10 mm (Device-1) and 20 mm (Device-2) were also constructed with similar procedure.

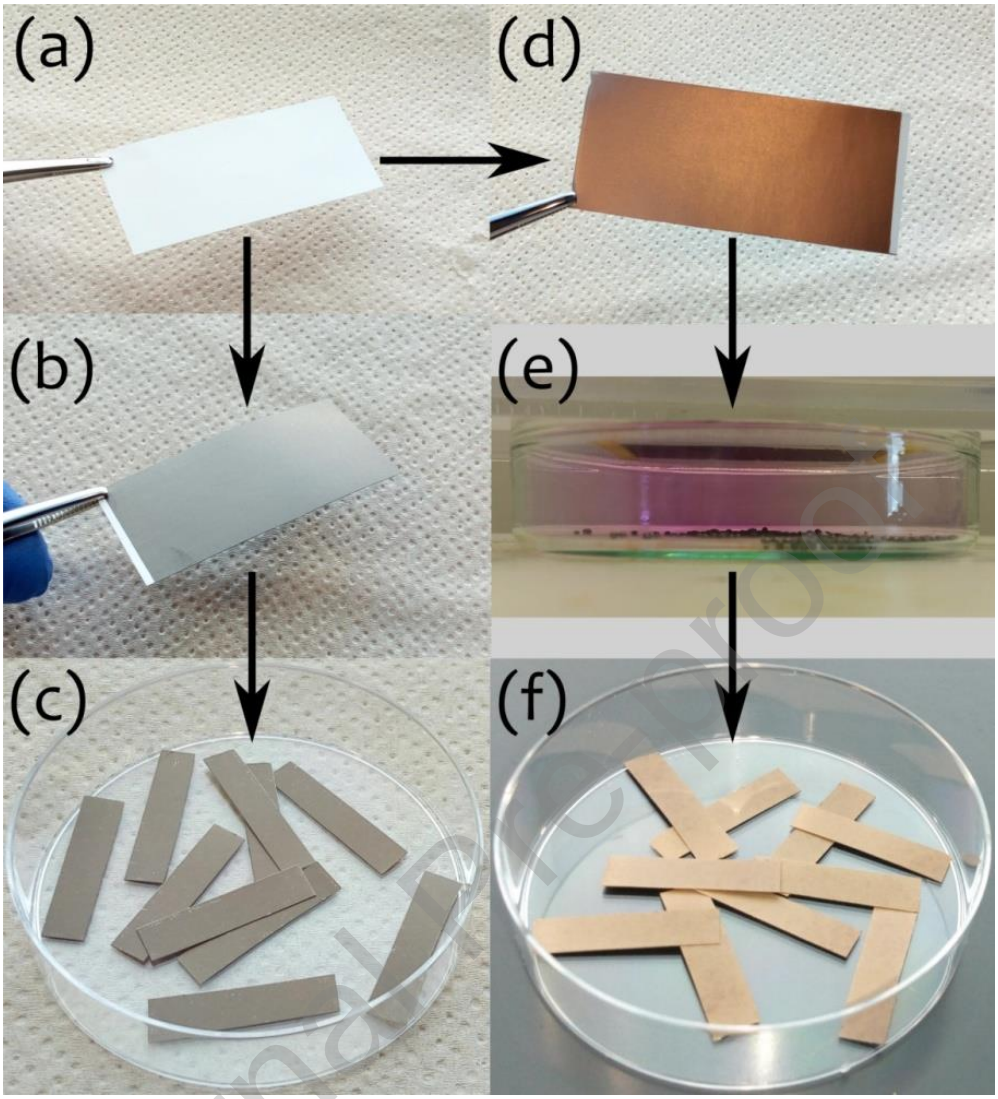

Figure 2. Photographs showing the cellulose paper used for deposition (a), as-sputtered Bi-coated paper before (b) and after being cut into strips (c), and Cu-sputtered paper prior to reaction with iodine vapour (d), during the iodination process (e) and following completion of the iodination and cutting steps (f).

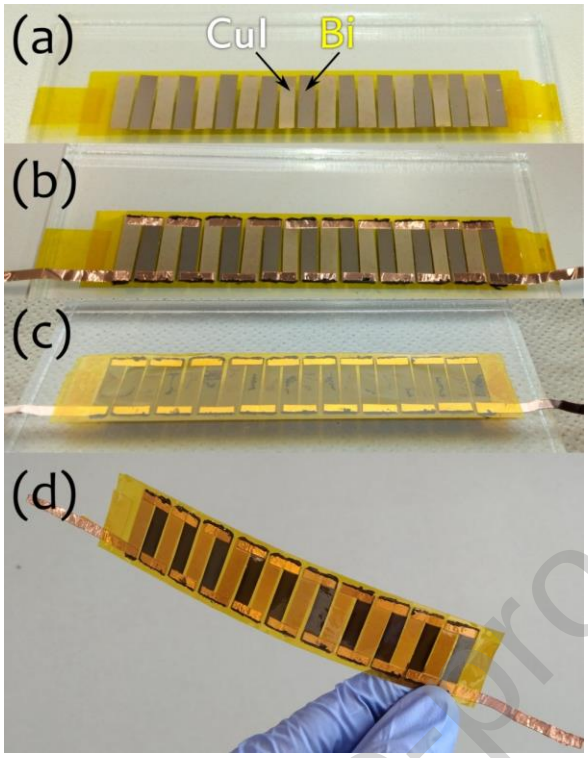

Figure 3. Sequential photographs depicting the process used to assemble the thermoelectric generators. After using high-temperature polyimide tape to secure ten pairs of alternating p- and n-type legs (Bi- and CuI-coated cellulose paper strips, respectively) in position (a), electrical connections between the legs were formed with conductive carbon paste and copper tape (b) and polyimide tape was applied to the top surface of the device to suppress air-exposure of the Bi and CuI films and increase physical stability (c); a completed device is pictured in (d).

Characterisation of the thin films

Measurements of the Seebeck coefficient and characterisation of morphology of the Bi and CuI films were carried out using as-coated 10 mm x 5 mm cellulose paper strips. The Seebeck coefficient was measured using a custom-built apparatus by applying a temperature difference (ΔT) along the length of each strip using built-in resistive heaters at the electrodes and measuring the generated thermoelectric voltage (ΔV) [39]. Temperatures were measured using k-type thermocouples and all the voltage readings were recorded using digital

multimeters (resolution 1 μV). The Seebeck coefficients of the films were estimated using the expression [40, 41]:

$$S = -\left(\frac{\Delta V}{\Delta T}\right) \qquad \text{……..(2)}$$

The electrical conductivity of the films was measured using the standard four-probe method; in a typical measurement, currents (I = 10-50 μA) were supplied through the outer probes and generated electrical potentials between inner probes were measured. The electrical conductivity (σ) of the samples was obtained using the following expression [42, 43]

$$\sigma = \frac{I}{V\ 2\pi s} \qquad \text{.....(3)}$$

where I is the applied current, V is the corresponding voltage, and s is the probe spacing; suitable correction factors were applied to obtain final values [43]. In the case of Bi-sputtered strips, the final thickness of each Bi film was assumed equal to 200 nm in conductivity calculations, in accordance with the thickness setting applied during Bi-sputtering. For CuI film, a thickness of 1.4 μm (estimated from cross-sectional scanning electron microscopy (SEM), Figure S1 (Supporting Information)) was used during estimation of the CuI conductivity.

The morphologies of the films were examined by scanning electron microscopy (SEM) using Zeiss Evo LS25 SEM, using an accelerating voltage of 20 kV and emission current of 20 μA. Powder X-ray diffraction (XRD) pattern of the CuI film was recorded in order to confirm its formation using a Bruker D8 Discover diffractometer with Cu Kα radiation, with a 2θ step size of 0.025° and dwell time of 0.5 s.

Thermoelectric testing of the generators

The thermoelectric performance of generators was investigated by fixing the devices on a hot-plate using polyimide tape and applying a temperature difference (ΔT) in the direction parallel to the n- and p-type legs, and digital multimeters (HMC 8012 DMM) were used to measure the open-circuit voltage (V_0) and short-circuit current (I_0) at different temperature

differences. The measurement setup is schematically illustrated in Figure S2 (Supporting Information). From these measurements, the maximum power output (P_{max}) was estimated using the standard expression,

$$P_{max} = \left(\frac{V_0 I_0}{4}\right) \quad \text{.....(4)}$$

which assumes a linear relationship between the generated voltage and current [44].

Stability of output voltage and current from the thin film devices is also important when they are used under bending or flexible modes. The reliability of a device (L20) outputs were tested after bending it for multiple times as illustrated in Figure S3 (Supporting Information). Subsequently, its performance under a curved mode was investigated by mounting onto the surface of a curved hot surface (a 1L beaker filled with hot water) and measuring its outputs. The device was firmly fixed on the beaker surface using polyimide tape by creating a direct contact of the device's topside whereas the bottom side was away from the beaker surface which was achieved from an insulating separator strip (thickness ~1mm) attached on the bottom side of the device in order to achieve temperature difference along the thermoelectric legs, and its output voltages were measured at two different temperatures of water.

Results and Discussion

As shown by the SEM images in Figure 4, the as-deposited Cu and Bi films appeared morphologically homogeneous across the examined surface of the cellulose paper. Furthermore, CuI films obtained after vapour iodination of sputtered Cu seemingly had a smoother surface than the Cu films from which they formed. The conversion of Cu into CuI was confirmed through XRD analysis of the CuI deposited paper substrate (Figure S4 (Supporting Information)); the pattern has all the peaks that match with the standard structure of cubic phase CuI (JCPDS File No. 06-0246).

Before testing thermoelectric devices, the thermoelectric properties of individual CuI and Bi paper strips were examined by thermoelectric measurements. The Seebeck coefficient (*S*), electrical conductivity (σ), and power factor (*PF*) data are shown in Figure 5; with S = 140 μV $K^{-1}$and σ = 28.1 S cm^{-1}, the *PF* of CuI film was estimated as ~56 μW m^{-1} K^{-2} (at 30 °C). The value of *S* was found to increase with increasing measurement temperature, yielding a maximum *PF* of ~65 μW m^{-1} K^{-2} at 80 °C. For the Bi film, the values were fairly stable over the measured temperature range with S = -45 μV K^{-1} and σ = 1.58 x 10^2 S cm^{-1} at room temperature, producing a *PF* of ~31 μW m^{-1} K^{-2}. A list of properties is summarized in Table I.

Table I. Summary of properties of CuI and Bi thin films used in the fabrication of the devices.

Sample	**Film thickness**	**Seebeck coefficient**	**Electrical conductivity**	**Power factor (at 30 °C)**
CuI film	1.4 μm	140 μV K^{-1}	28.1 S cm^{-1}	56 μW m^{-1} K^{-2}
Bi film	200 nm	-45 μV K^{-1}	1.58 x 10^2 S cm^{-1}	31 μW m^{-1} K^{-2}

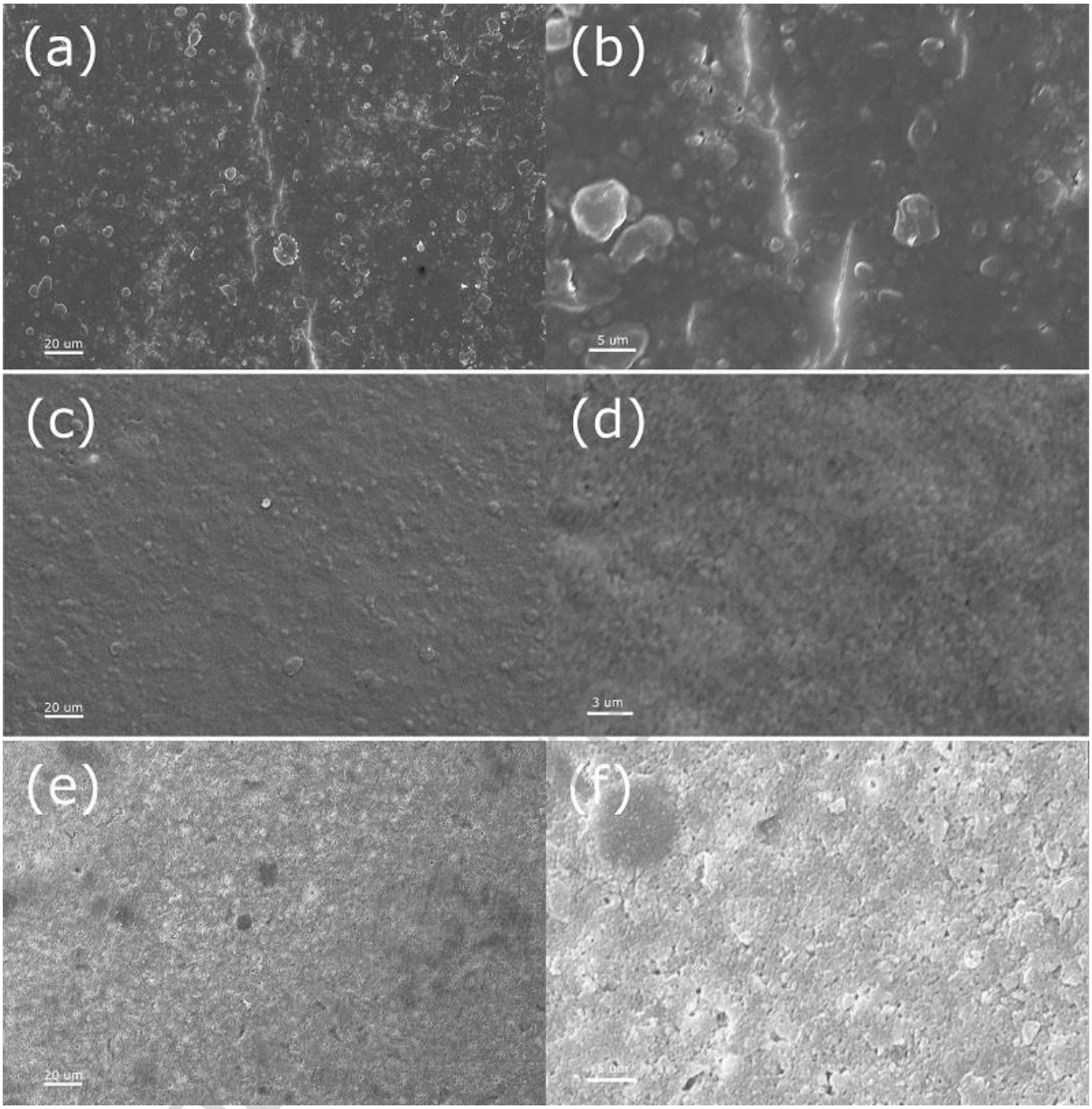

Figure 4. SEM images of Cu-coated cellulose paper (a-b), CuI films fabricated via vapour iodination of Cu films (c-d), and Bi-coated cellulose paper (e-f).

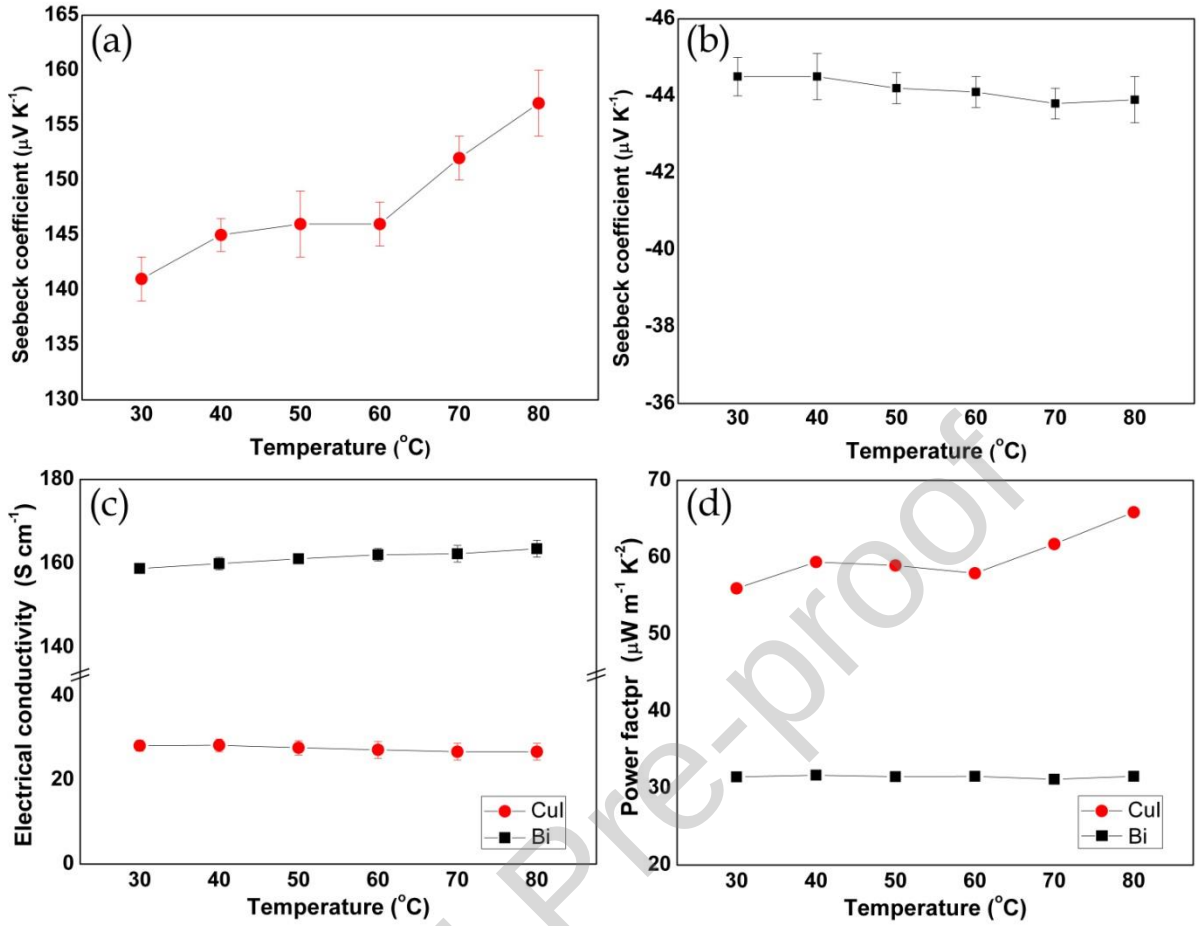

Figure 5. Measured temperature-dependent Seebeck coefficient of CuI (a), and Bi (b), alongside corresponding changes in the electrical conductivity (c) and power factor (d).

When thermoelectric legs are exposed to a temperature gradient ($\Delta T = T_h - T_c$, where T_h and T_c are hot and cold side temperatures of the legs), they generate an electrical potential (ΔV) of magnitude dependent on the Seebeck coefficient (S) of the leg and the temperature gradient (ΔT) along it, according to the expression [45].

$$\Delta V = -S\,\Delta T \qquad \text{.....(5)}$$

Thus, ΔV is practically limited by the maximum temperature gradient that can be maintained over the length of the leg, which is in turn dependent on both its length and the thermal conductivity of the thermoelectric material. As shown by Figure 6a, the open-circuit voltage (V_0) and short-circuit current (I_0) increased linearly with applied ΔT, with V_0 and I_0 reaching maximum values of 87.5 ± 1.2 mV and 3.7 ± 0.2 μA at ΔT = 49 K, respectively; substituting

these quantities into Equation (4), one obtains a corresponding P_{max} value of 80.9 ± 4.5 nW. From the plotted linear fit of the $V_0(\Delta T)$ relationship, a Seebeck coefficient of 1.81 mV K^{-1} is estimated for the device, or 181 µV K^{-1} for each p-n pair; this value is in close agreement with the sum of individual contributions from one p-type CuI leg (S = ~ 140-155 µV K^{-1}) and one n-type Bi leg (S = ~ -45 µV K^{-1}), equal to185-200 µV K^{-1}.

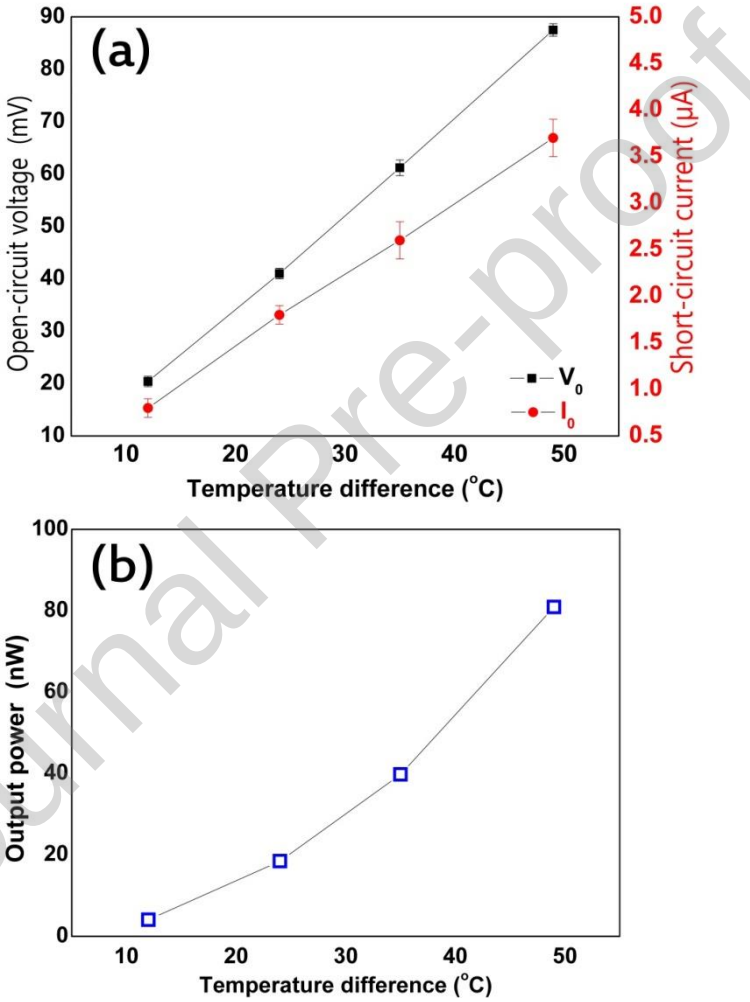

Figure 6. Output performance characteristics of the ten pair device (L20), including measured relationships between the open-circuit voltage (V_0), short-circuit current (I_0) and the temperature gradient (ΔT) in the direction parallel to the p-n legs (a), and the estimated maximum power (P_{max}) as a function of ΔT (b).

A key asset of the present thermoelectric generator design is its flexibility, which enables its use in applications involving curved or uneven surfaces. To illustrate this point,

the as-prepared device (L20) was mounted onto the surface of a 1L beaker filled with hot water; a photograph of this setup is shown in Figure 7, alongside a graph depicting the measured output voltage at different water temperatures. The output voltages measured at temperatures of 40 ºC and 60 ºC were 21 ± 0.8 mV and 38 ± 1.5 mV, respectively; although these values are lower than expected from Figure 6, one may reasonably account for the discrepancies by noting that the temperature of the outer beaker surface was likely marginally lower than the measured temperature of the water.

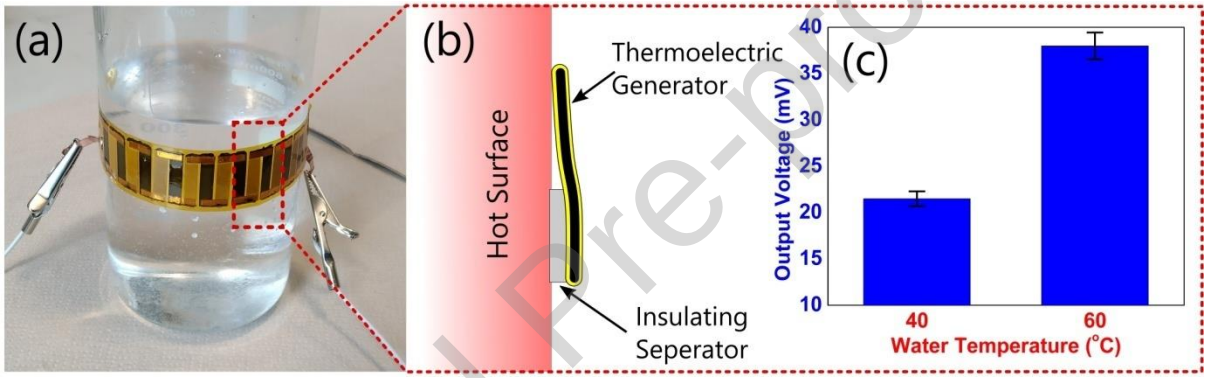

Figure 7. Photograph showing the application of the thermoelectric generator to utilise thermal energy from the curved surface of a heated beaker (a), a schematic side-view illustration of the junction between the beaker and the device (b), and a graph plotting the measured output voltage at water temperatures of 40 ºC and 60 ºC (c). As depicted within the illustration, an insulating separator was situated between the beaker and the bottom end of the device in order to attain a temperature difference between the ends of each thermoelectric leg.

When bending a thermoelectric generator to suit a given surface topography, it is crucial that its performance does not deteriorate as a result of the deformation. As shown graphically in Figure S3 (Supporting Information), which also depicts various stages during bending of the thermoelectric generator, the open-circuit voltage measured at a temperature difference of 35 ºC decreased by only 1.5% after 50 successive bending cycles, whilst short-

circuit current diminished by 7.5% over the same sequence. However, following a further 50 bending cycles there was negligible variation in the output characteristics, suggesting that the initial deterioration resulted from cracks that formed during early bending cycles. The Kapton tape has a major role in maintaining physical stability of the device during such bendings.

In order to maximise the power produced by a thermoelectric generator, it is important to suppress resistive losses by minimising the length of each thermoelectric leg. However, maintaining a given temperature difference between the two ends of a thermoelectric leg becomes increasingly difficult as the length of the leg is decreased, as the maximum sustainable temperature gradient is limited by the thermal conductivities of the thermoelectric material and the underlying substrate. To address these considerations in the context of the present thermoelectric generator design, a one-pair device with reduced leg length (Device-1)was tested and the open-circuit voltage across the device was measured for a period of thirty minutes at a temperature difference of ca. 30 ºC, as plotted in Figure 8. From the stability of the voltage output it is clear that the temperature gradient across the device reached a sustainable equilibrium during the experiment, indicating that the shortened legs did not inhibit the ability of the system to operate under this temperature condition.

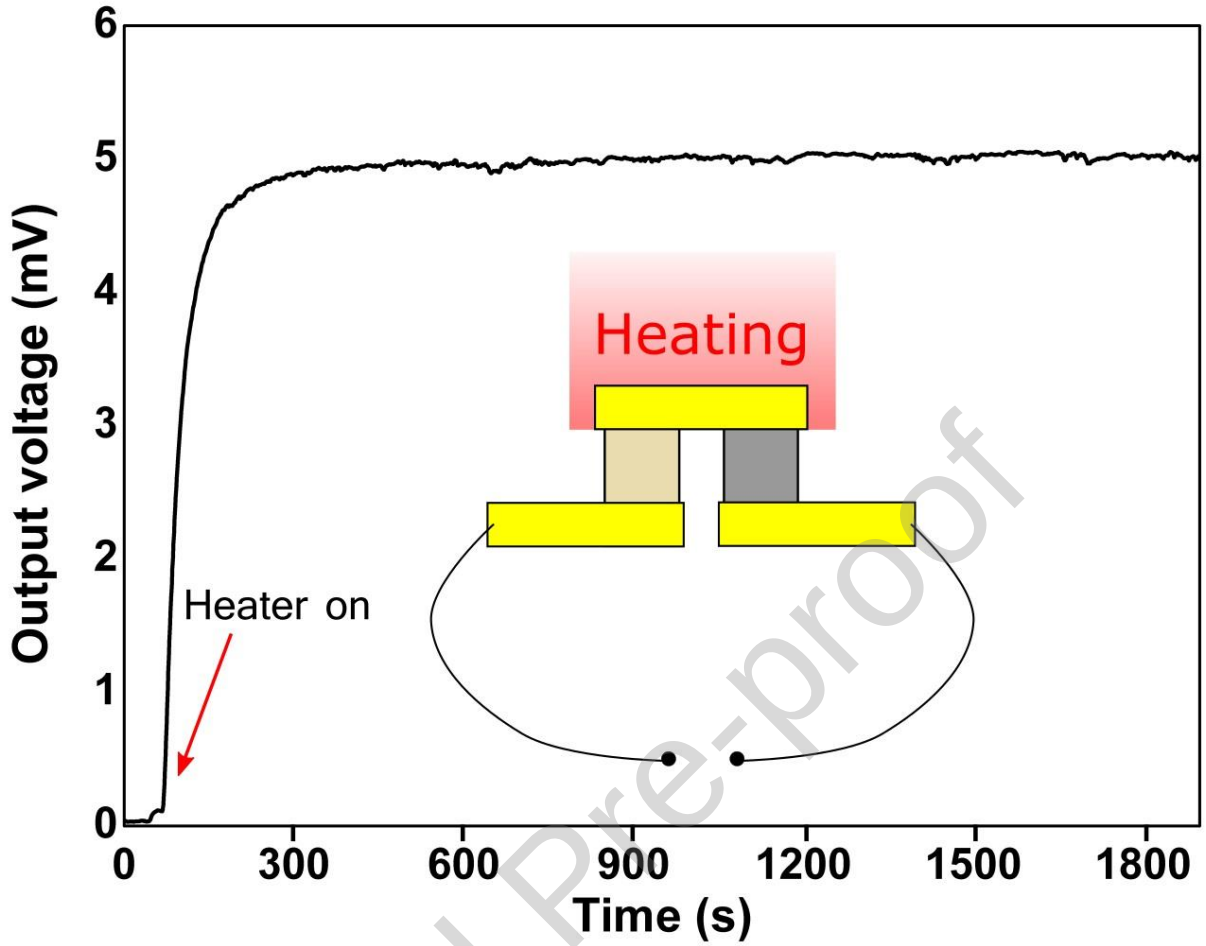

Figure 8. Stability of open circuit voltage from the one-pair device (Device-1) under a constant heating at one side (50 ºC).

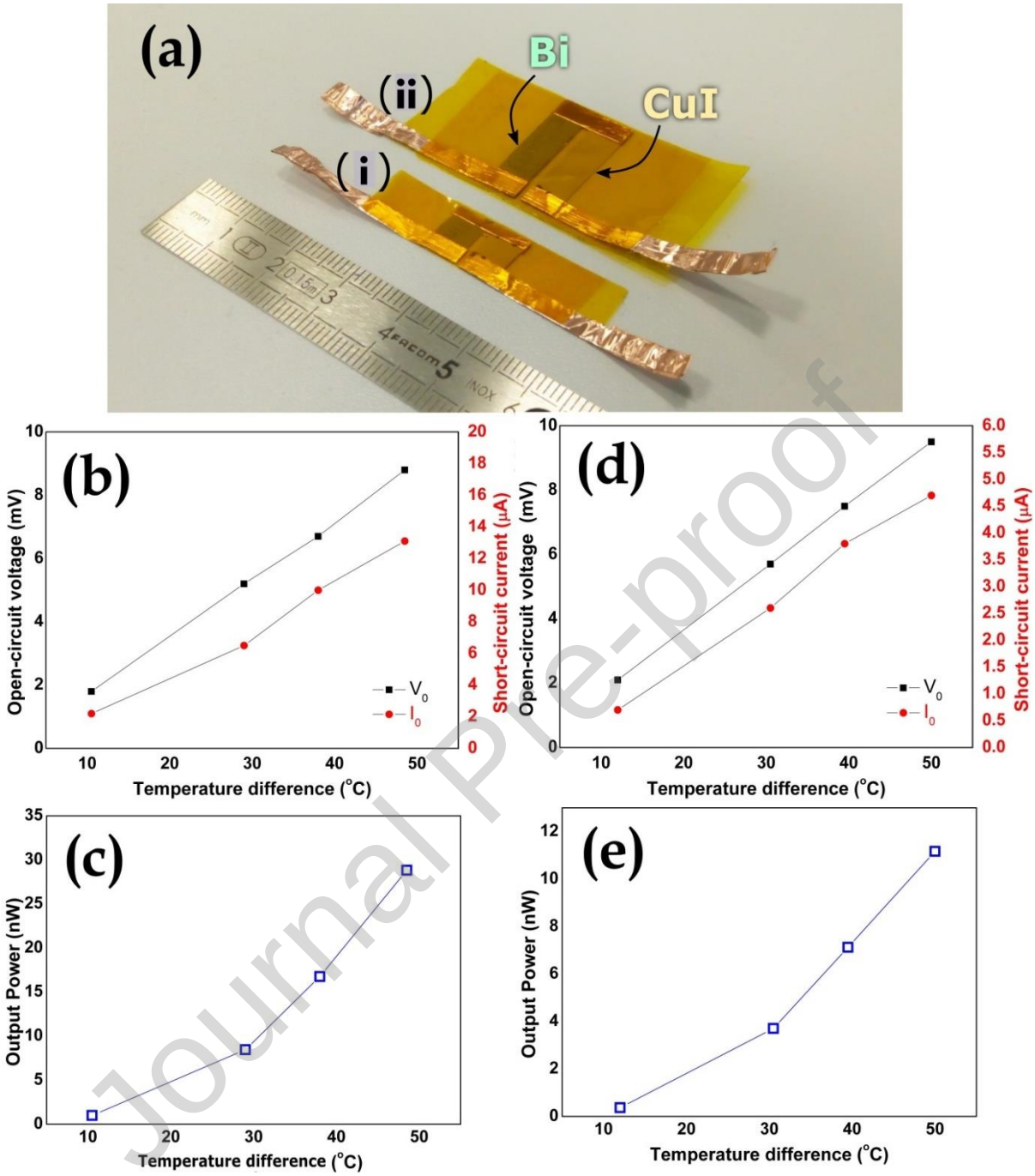

Figure 9. Photograph of one-pair devices (a) Device-1 (i) and Device-2 (ii), in addition to plots depicting their output performance: plot (b) shows the variation of open-circuit voltage (V_0) and short-circuit current (I_0) from the Device-1 as functions of temperature difference, with the estimated maximum output power (P_{max}) of the system plotted in (c), whilst plot (d) displays the corresponding variations of V_0 and I_0 from the Device-2 alongside the associated relationship between P_{max} and hot-side temperature (e).

A comparison of one-pair devices of two different leg lengths is provided by Figure 9, which displays the measured variations of V_0 and I_0 from the photographed systems as functions of temperature difference, in addition to the corresponding P_{max} estimates obtained from Eq. (4). Whilst the two devices produced similar V_0 measurements across the investigated temperature range, the Device-1 yielded I_0 values that were over two times those of its Device-2. Consequently, P_{max} estimates from the Device-1 significantly exceeded the corresponding values associated with the Device-2, with the former reaching 28 nW at a temperature difference of ca. 50 ºC in comparison to 11 nW in the latter case. One may rationalise this result by recognising that decreasing the length of each thermoelectric leg leads to a corresponding reduction in series resistance, thereby enhancing I_0 in accordance with the expression[46]

$$I_0 = \frac{S_{pn}\,\Delta T}{R_{int}} \qquad \text{..... (6)}$$

where S_{pn} is the total Seebeck coefficient of the one-pair p-n junction or device, ΔT is the applied temperature difference, and R_{int} is the internal resistance of the device. It follows from Eq. (4) that one may further enhance the thermoelectric performance by increasing the number of junctions within the device. In order to address this point, a ten-pair thermoelectric generator (L10) with reduced leg length was characterised under applied ΔT values of 10-50 ºC; V_0 and I_0 measurements acquired over this range are plotted in Figure 10a, with corresponding P_{max} estimates displayed as a function of ΔT in Figure 10b.Whilst the V_0 values yielded by this device are similar to those obtained from the L20 device, as displayed previously in Figure 6a, reduction of the leg length once again resulted in a significant enhancement in I_0; for instance, with ΔT set to 49 ºC, the L10 device produced 10.2 μA under short-circuit conditions, which is almost three times the 3.7 μA exhibited by the L20 device. Accordingly, the L10 configuration was capable of providing an estimated maximum power of 215 nW at a 49 ºC temperature difference, representing a considerable improvement with

respect to the L20 device, for which a corresponding P_{max} value of 80 nW was estimated. Furthermore, it should be noted that the power estimates shown in Figure 10b are comparable, and in many cases superior, to the maximum power characteristics of planar devices reported elsewhere in the literature, which are typically fabricated using expensive and toxic thermoelectric materials [47-49]: Table II compares the maximum power estimate at a ΔT value of 49 ºC with the thermoelectric power outputs from a representative selection of these literature prototypes.

Theoretically estimated device output voltage, current, and power outputs are summarized in Table III, which shows that the estimated power output values are higher than the experimentally observed values. However, the experimental power outputs of one pair devices (Device-1 and Device-2) are in near agreement with the estimated values. There are more differences in the outputs of ten pair devices (L10 and L20), which is mainly arising from the theoretical estimation of the internal resistance of the ten pair devices for which the resistance of one pair devices was taken as a reference (For example, if the resistance of a one pair device is R then the resistance of a ten pair device is considered as 10R). But the actual/measured internal resistance of the ten pair devices was more than the estimated values because of the additional contact resistance from carbon conductive paint. The measured internal resistance values of the one pair devices were 0.71 kΩ (leg length ~10 mm) and 1.65 kΩ (leg length ~20 mm). Similarly, for ten pair devices, the internal resistance values were 7.35 kΩ (leg length ~10 mm) and 17.10 kΩ (leg length ~20 mm). Therefore, there can be many factors associated with such changes such as measurement errors, additional internal resistance of the devices due to electrical connections used in between the thermoelectric elements, lack of uniform heating of all the thermoelectric elements during the measurements, etc. For illustration, the difference in the experimentally observed output values and the estimated values can be minimized by achieving direct electrical contact

between the p-type and n-type films which avoids the use of conducting paints, as this approach minimizes the internal resistance of the resulting device.

Further, the stability in the performance of these devices with ageing was studied by testing one of the devices (Device-1) after 2, 7 and 15 days. A fixed temperature difference (30 ºC) was applied for every measurement in order to make comparison of the outputs. The data shown in Figure S5 (Supporting Information) suggests that the devices produce fairly stable outputs over time. However, a small increase in the output voltage at the expense of a small decrease in the current was observed after 7 days and both the voltage and current were quite stable thereafter as it can be observed from comparing results of day-7 and day-15. As a result, device's overall performance was quite similar and stable as it was in the beginning but with a small reduction of 1.3% in the power output. Further, a comparison between the power output stability of this Kapton covered and an uncovered one pair device has been made to observe the role of Kapton tape. Figure 11 shows the relative power outputs of the devices as a function of number of days, the data of which are all normalized to the output reading of the first day. In case of uncovered device, a reduction of 3.5% in the power output has been observed while it is 1.3% for the Kapton covered device, which indicates that Kapton protection layer can help maintain stable performance and also improves device's physical structure.

For real applications, these planar devices can be directly fixed on a hot surface with an insulating separator strip on one side of the thermoelectric elements as illustrated in Figure 7, where the device was directly fixed on a hot beaker to demonstrate its working. To achieve a good physical contact between the hot surface and the device, high temperature adhesive tapes such as Kapton tapes can be used to mount the devices on the desired surface. Further, the number of thermoelectric elements should be increased to get higher power outputs from the devices. Overall, materials like CuI with attractive thermoelectric properties and low-

toxicity can help build simple and low-cost devices that can be used for low-grade heat conversion applications.

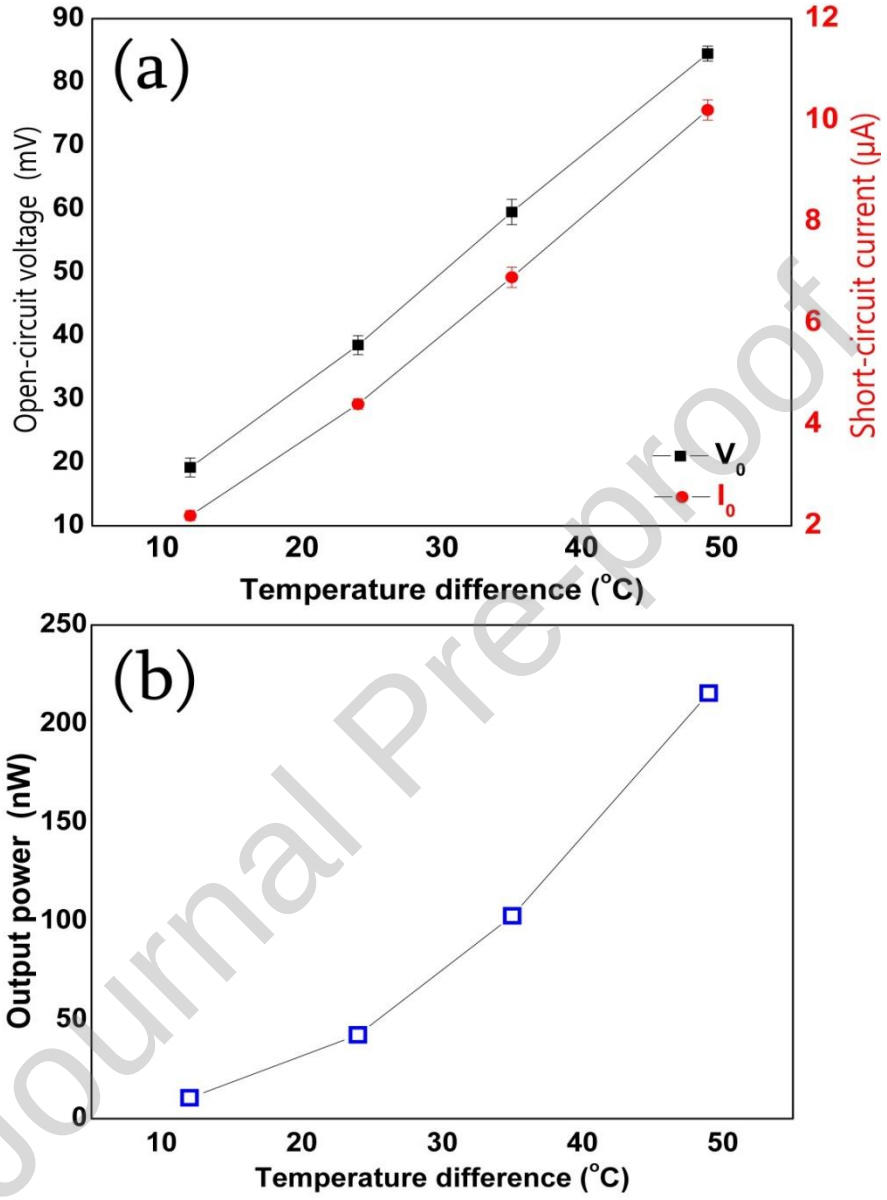

Figure 10. Measured relationships between the open-circuit voltage (V_0), short-circuit current (I_0) and end-to-end temperature difference (ΔT) from a ten-pair thermoelectric generator (L10) (a), in addition to corresponding maximum power estimates (P_{max}) as a function of ΔT (b).

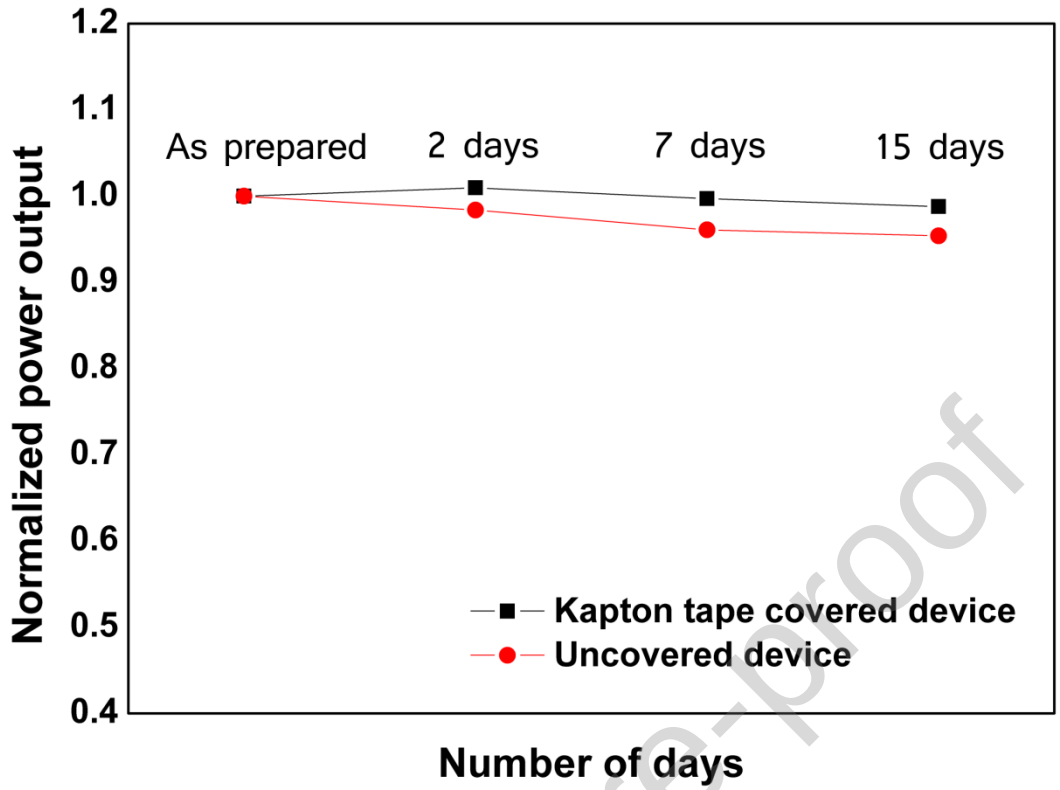

Figure 11. Normalized power outputs of a Kapton covered and uncovered one pair device over time. The output data are all normalized to the output readings of the first day of respective device.

Table II. Voltage and power outputs comparison of the present device with the reported planar generators.

Thermoelectric materials	**Number of p-n pairs**	**Temperature difference (K)**	**Open-circuit voltage (mV)**	**Maximum power (nW)**	**Normalised open circuit voltage ($\mu V\ K^{-1}\ pair^{-1}$)**	**Normalised maximum power ($nW\ K^{-1}\ pair^{-1}$)**	**Reference**
p-type CuI & n-type Bi	10	49	84.5	215	172	0.439	This work
p-type CuI & n-type GZO (Gallium-doped zinc oxide)	17	20	35	11	103	0.032	[50]
p-type Sb_2Te_3 & n-type Bi_2Te_3	15	35	210	700	400	1.333	[38]
p-type Sb_2Te_3 & n-	20	50	300	353			[51]

type Bi_2Te_3					300	0.353	
p-type Sb_2Te_3 & n-type Bi_2Te_3	100	40	430	32	107	0.008	[48]
p-type Sb_2Te_3 & n-type Bi_2Te_3	242	22	294	5,900	55	1.108	[52]
p-type SnTe & n-typePbTe	4	120	250	366	521	0.762	[53]
p-type $NbSe_2$ & n-type WS_2	100	60	--	38	--	-- 0.006	[54]

Table III. Summary of theoretically estimated device properties and comparison with experimentally measured power output values. The internal resistance of one pair devices have been used to estimate the internal resistance of the corresponding ten pair devices (For ex. Device-1: R_{int} = 0.71 kΩ; for ten pair device R_{int} = 0.71 kΩ x 10 pairs = 7.1 kΩ). The Seebeck coefficient of 1 p-n pair, S_{pair}= (S_{CuI} + S_{Bi}) =185 µV/K; S_{CuI} =140 µV/K, S_{Bi} = -45 µV/K.

Device details	Number of p-n pairs	Seebeck coefficient of one p-n pair (S_{pair}) (µV/K)	Estimated open circuit voltage (V_o=S_{pair} x ΔT) at ΔT=49 K (mV)	Internal resistance (R_{int}) of the device (kΩ)	Estimated Short-circuit current (I_o=S_{pair} x ΔT/R_{int}) (µA)	Estimated power output at ΔT=49 K (nW)	Measured power output at ΔT=49 K (nW)
Device-1 (leg length ~10 mm)	1	185	9.06	0.71	12.8	29	28
Device-L10 (leg length ~10 mm)	10	185	90.6	7.1	12.8	290	215
Device-2 (leg length ~20 mm)	1	185	9.06	1.65	5.5	12.5	11
Device-L20 (leg length ~20 mm)	10	185	90.6	16.5	5.5	125	80

Conclusions

This work presents a simplified method for fabricating thermoelectric devices with promising output powers and physical stability. The chosen p-type material, CuI, is a well-suited material for designing cellulose paper based devices from which higher thermal gradients can be achieved even at low temperature heating, which in turn result in higher power outputs. Further improvements in the device performance are possible by using better electrical connections between the legs or by directly connecting the CuI and Bi films to avoid unnecessary electrical connections between them. Overall the cellulose paper based devices securely packaged inside thermally stable layers like Kapton tape can have better life time and stability. Such devices can be very simple to design and fabricate, and are low-cost and suitable for low-grade waste heat recovery.

Acknowledgments

Authors are thankful to the Welsh Government (EU European Regional Development Fund) for funding the Rice (Reducing Industrial Carbon Emission) project (Grant Number: 81435). Authors would like to acknowledge the assistance provided by Swansea University College of Engineering AIM Facility, which was funded in part by the EPSRC (EP/M028267/1), the European Regional Development Fund through the Welsh Government (80708) and the Ser Solar project via Welsh Government.

Conflict of Interest

The authors declare no conflict of interest.

Data availability

Data that support the findings are available in the supplementary information of the manuscript.

References:

[1] G.J. Meyer, K. Biswas, A Special Forum Issue on Thermoelectric Energy Conversion, ACS Applied Energy Materials 3(3) (2020) 2037-2038.
[2] C. Forman, I.K. Muritala, R. Pardemann, B. Meyer, Estimating the global waste heat potential, Renewable and Sustainable Energy Reviews 57 (2016) 1568-1579.
[3] G.J. Snyder, E.S. Toberer, Complex thermoelectric materials, Nature Materials 7(2) (2008) 105-114.
[4] R. Mulla, C.W. Dunnill, Powering the Hydrogen Economy from Waste Heat: A Review of Heat-to-Hydrogen Concepts, ChemSusChem 12(17) (2019) 3882-3895.
[5] X. Li, L. Zhao, J. Yu, X. Liu, X. Zhang, H. Liu, W. Zhou, Water Splitting: From Electrode to Green Energy System, Nano-Micro Letters 12(1) (2020) 131.
[6] X. Zhang, W. Gao, X. Su, F. Wang, B. Liu, J.-J. Wang, H. Liu, Y. Sang, Conversion of solar power to chemical energy based on carbon nanoparticle modified photo-thermoelectric generator and electrochemical water splitting system, Nano Energy 48 (2018) 481-488.
[7] R. Phillips, Charles W. Dunnill, Zero gap alkaline electrolysis cell design for renewable energy storage as hydrogen gas, RSC Advances 6(102) (2016) 100643-100651.
[8] J.A.R. Katherine Glover, Daniel R Jones, Elaine Forde, Michael EA Warwick, William Gannon, Charles W Dunnill, The Hydrogen Bike: Communicating the Production and Safety of Green Hydrogen, Frontiers in Communication 5 (2020) 138.
[9] W. Liu, X. Yan, G. Chen, Z. Ren, Recent advances in thermoelectric nanocomposites, Nano Energy 1(1) (2012) 42-56.
[10] M.R. Burton, S. Mehraban, D. Beynon, J. McGettrick, T. Watson, N.P. Lavery, M.J. Carnie, 3D Printed SnSe Thermoelectric Generators with High Figure of Merit, Advanced Energy Materials 9(26) (2019) 1900201.
[11] M.R. Burton, T. Liu, J. McGettrick, S. Mehraban, J. Baker, A. Pockett, T. Watson, O. Fenwick, M.J. Carnie, Thin Film Tin Selenide (SnSe) Thermoelectric Generators Exhibiting Ultralow Thermal Conductivity, Advanced Materials 30(31) (2018) 1801357.
[12] F.F. Jaldurgam, Z. Ahmad, F. Touati, Synthesis and Performance of Large-Scale Cost-Effective Environment-Friendly Nanostructured Thermoelectric Materials, Nanomaterials 11(5) (2021).
[13] L.S. Hewawasam, A.S. Jayasena, M.M.M. Afnan, R.A.C.P. Ranasinghe, M.A. Wijewardane, Waste heat recovery from thermo-electric generators (TEGs), Energy Reports 6 (2020) 474-479.
[14] R. Freer, A.V. Powell, Realising the potential of thermoelectric technology: a Roadmap, Journal of Materials Chemistry C 8(2) (2020) 441-463.
[15] R. Mulla, C.W. Dunnill, Graphite-loaded cotton wool: A green route to highly-porous and solid graphite pellets for thermoelectric devices, Composites Communications 20 (2020) 100345.
[16] N. Jaziri, A. Boughamoura, J. Müller, B. Mezghani, F. Tounsi, M. Ismail, A comprehensive review of Thermoelectric Generators: Technologies and common applications, Energy Reports 6 (2020) 264-287.
[17] G. Kogo, B. Xiao, S. Danquah, H. Lee, J. Niyogushima, K. Yarbrough, A. Candadai, A. Marconnet, S.K. Pradhan, M. Bahoura, A thin film efficient pn-junction thermoelectric device fabricated by self-align shadow mask, Scientific Reports 10(1) (2020) 1067.
[18] Y. Du, J. Chen, Q. Meng, J. Xu, J. Lu, B. Paul, P. Eklund, Flexible Thermoelectric Double-Layer Inorganic/Organic Composites Synthesized by Additive Manufacturing, Advanced Electronic Materials 6(8) (2020) 2000214.
[19] X. Chen, Z. Zhou, Y.-H. Lin, C. Nan, Thermoelectric thin films: Promising strategies and related mechanism on boosting energy conversion performance, Journal of Materiomics 6(3) (2020) 494-512.
[20] Y. Du, J. Xu, B. Paul, P. Eklund, Flexible thermoelectric materials and devices, Applied Materials Today 12 (2018) 366-388.

[21] R. Mulla, D.R. Jones, C.W. Dunnill, Thermoelectric Paper: Graphite Pencil Traces on Paper to Fabricate a Thermoelectric Generator, Advanced Materials Technologies 5(7) (2020) 2000227.
[22] M.S. Hossain, T. Li, Y. Yu, J. Yong, J.-H. Bahk, E. Skafidas, Recent advances in printable thermoelectric devices: materials, printing techniques, and applications, RSC Advances 10(14) (2020) 8421-8434.
[23] S. LeBlanc, S.K. Yee, M.L. Scullin, C. Dames, K.E. Goodson, Material and manufacturing cost considerations for thermoelectrics, Renewable and Sustainable Energy Reviews 32 (2014) 313-327.
[24] R. Mulla, D.R. Jones, C.W. Dunnill, Economical and Facile Route to Produce Gram-Scale and Phase-Selective Copper Sulfides for Thermoelectric Applications, ACS Sustainable Chemistry & Engineering 8(37) (2020) 14234-14242.
[25] R. Mulla, M.K. Rabinal, Large-scale synthesis of copper sulfide by using elemental sources via simple chemical route, Ultrasonics Sonochemistry 39 (2017) 528-533.
[26] C. Yang, D. Souchay, M. Kneiß, M. Bogner, H.M. Wei, M. Lorenz, O. Oeckler, G. Benstetter, Y.Q. Fu, M. Grundmann, Transparent flexible thermoelectric material based on non-toxic earth-abundant p-type copper iodide thin film, Nature Communications 8(1) (2017) 16076.
[27] N. Yamada, R. Ino, Y. Ninomiya, Truly Transparent p-Type γ-CuI Thin Films with High Hole Mobility, Chemistry of Materials 28(14) (2016) 4971-4981.
[28] R. Mulla, M.K. Rabinal, Defect-Controlled Copper Iodide: A Promising and Ecofriendly Thermoelectric Material, Energy Technology 6(6) (2018) 1178-1185.
[29] B.M. Morais Faustino, D. Gomes, J. Faria, T. Juntunen, G. Gaspar, C. Bianchi, A. Almeida, A. Marques, I. Tittonen, I. Ferreira, CuI p-type thin films for highly transparent thermoelectric p-n modules, Scientific reports 8(1) (2018) 6867-6867.
[30] H.J. Goldsmid, Bismuth -- The Thermoelectric Material of the Future?, 2006 25th International Conference on Thermoelectrics, 2006, pp. 5-10.
[31] W. Wei, Z. Weiling, S. Liping, Z. Jianzhong, G. Jianping, Fabrication of thermoelectric materials with bismuth nanowire array, Proceedings ICT2001. 20 International Conference on Thermoelectrics (Cat. No.01TH8589), 2001, pp. 367-370.
[32] M. Rafiq, D.C. W, Fabrication of wooden thermoelectric legs to construct a generator, Green Materials 0(0) 1-8.
[33] G. Dombek, Z. Nadolny, P. Przybylek, R. Lopatkiewicz, A. Marcinkowska, L. Druzynski, T. Boczar, A. Tomczewski, Effect of Moisture on the Thermal Conductivity of Cellulose and Aramid Paper Impregnated with Various Dielectric Liquids, Energies 13(17) (2020).
[34] M.M.R.A. Lima, R.C.C. Monteiro, M.P.F. Graça, M.G. Ferreira da Silva, Structural, electrical and thermal properties of borosilicate glass–alumina composites, Journal of Alloys and Compounds 538 (2012) 66-72.
[35] A. Ben-Yakar, A. Harkin, J. Ashmore, R.L. Byer, H.A. Stone, Thermal and fluid processes of a thin melt zone during femtosecond laser ablation of glass: the formation of rims by single laser pulses, Journal of Physics D: Applied Physics 40(5) (2007) 1447-1459.
[36] C. Qian, J. Sun, J. Yang, Y. Gao, Flexible organic field-effect transistors on biodegradable cellulose paper with efficient reusable ion gel dielectrics, RSC Advances 5(19) (2015) 14567-14574.
[37] R. Mulla, C.W. Dunnill, Single material thermocouples from graphite traces: Fabricating extremely simple and low cost thermal sensors, Carbon Trends 4 (2021) 100077.
[38] E.M.F. Vieira, A.L. Pires, J.P.B. Silva, V.H. Magalhães, J. Grilo, F.P. Brito, M.F. Silva, A.M. Pereira, L.M. Goncalves, High-Performance µ-Thermoelectric Device Based on Bi2Te3/Sb2Te3 p–n Junctions, ACS Applied Materials & Interfaces 11(42) (2019) 38946-38954.
[39] R. Mulla, M.K. Rabinal, A Simple and Portable Setup for Thermopower Measurements, ACS Combinatorial Science 18(4) (2016) 177-181.
[40] R. Mulla, K. Glover, C.W. Dunnill, An Easily Constructed and Inexpensive Tool to Evaluate the Seebeck Coefficient, IEEE Transactions on Instrumentation and Measurement 70 (2021) 1-7.
[41] R. Mulla, M.K. Rabinal, A tweezer as a thermoelectric tester, Physics Education 54(5) (2019) 055032.

[42] I. Miccoli, F. Edler, H. Pfnür, C. Tegenkamp, The 100th anniversary of the four-point probe technique: the role of probe geometries in isotropic and anisotropic systems, Journal of Physics: Condensed Matter 27(22) (2015) 223201.
[43] M.-Y. Li, M. Yang, E. Vargas, K. Neff, A. Vanli, R. Liang, Analysis of variance on thickness and electrical conductivity measurements of carbon nanotube thin films, Measurement Science and Technology 27(9) (2016) 095004.
[44] P. Fan, Z.-h. Zheng, Y.-z. Li, Q.-y. Lin, J.-t. Luo, G.-x. Liang, X.-m. Cai, D.-p. Zhang, F. Ye, Low-cost flexible thin film thermoelectric generator on zinc based thermoelectric materials, Applied Physics Letters 106(7) (2015) 073901.
[45] J.D. Ryan, A. Lund, A.I. Hofmann, R. Kroon, R. Sarabia-Riquelme, M.C. Weisenberger, C. Müller, All-Organic Textile Thermoelectrics with Carbon-Nanotube-Coated n-Type Yarns, ACS Applied Energy Materials 1(6) (2018) 2934-2941.
[46] S. Ferhat, C. Domain, J. Vidal, D. Noël, B. Ratier, B. Lucas, Organic thermoelectric devices based on a stable n-type nanocomposite printed on paper, Sustainable Energy & Fuels 2(1) (2018) 199-208.
[47] J.P. Rojas, D. Conchouso, A. Arevalo, D. Singh, I.G. Foulds, M.M. Hussain, Paper-based origami flexible and foldable thermoelectric nanogenerator, Nano Energy 31 (2017) 296-301.
[48] L. Francioso, C.D. Pascali, I. Farella, C. Martucci, P. Cretì, P. Siciliano, A. Perrone, Flexible thermoelectric generator for wearable biometric sensors, SENSORS, 2010 IEEE, 2010, pp. 747-750.
[49] Z. Lu, H. Zhang, C. Mao, C.M. Li, Silk fabric-based wearable thermoelectric generator for energy harvesting from the human body, Applied Energy 164 (2016) 57-63.
[50] J. Coroa, B.M. Morais Faustino, A. Marques, C. Bianchi, T. Koskinen, T. Juntunen, I. Tittonen, I. Ferreira, Highly transparent copper iodide thin film thermoelectric generator on a flexible substrate, RSC Advances 9(61) (2019) 35384-35391.
[51] F. Yang, S. Zheng, H. Wang, W. Chu, Y. Dong, A thin film thermoelectric device fabricated by a self-aligned shadow mask method, Journal of Micromechanics and Microengineering 27(5) (2017) 055005.
[52] M.-Y. Kim, T.-S. Oh, Thermoelectric Power Generation Characteristics of a Thin-Film Device Consisting of Electrodeposited n-Bi2Te3 and p-Sb2Te3 Thin-Film Legs, Journal of Electronic Materials 42(9) (2013) 2752-2757.
[53] V. Karthikeyan, J.U. Surjadi, J.C.K. Wong, V. Kannan, K.-H. Lam, X. Chen, Y. Lu, V.A.L. Roy, Wearable and flexible thin film thermoelectric module for multi-scale energy harvesting, Journal of Power Sources 455 (2020) 227983.
[54] J.Y. Oh, J.H. Lee, S.W. Han, S.S. Chae, E.J. Bae, Y.H. Kang, W.J. Choi, S.Y. Cho, J.-O. Lee, H.K. Baik, T.I. Lee, Chemically exfoliated transition metal dichalcogenide nanosheet-based wearable thermoelectric generators, Energy & Environmental Science 9(5) (2016) 1696-1705.

Graphical abstract

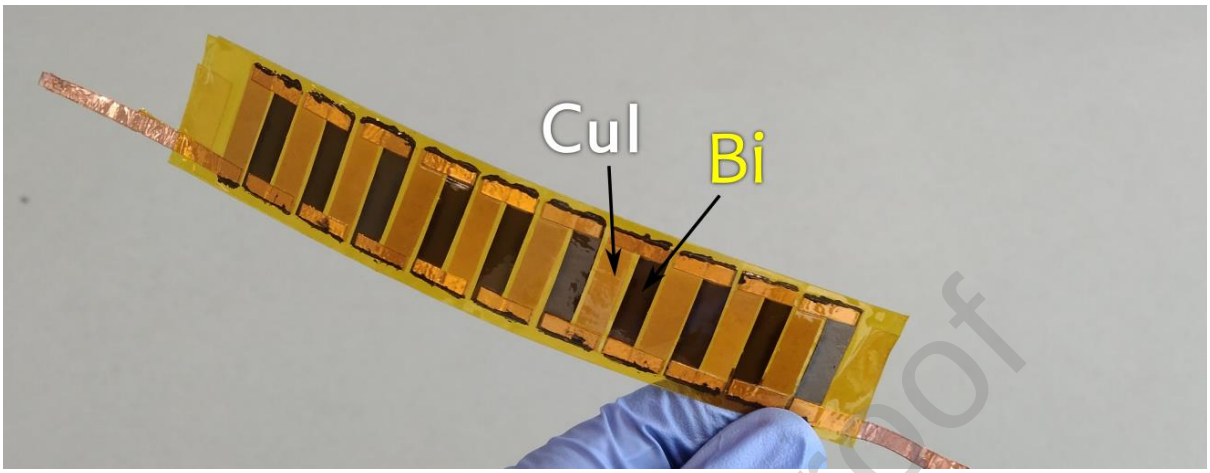

Author statement

Rafiq Mulla: Writing - original draft, Conceptualization, Methodology, Investigation, Validation.

Daniel R. Jones: Writing - review & editing, Validation.

Charles W. Dunnill: Supervision, Writing - review & editing, Resources, Project administration, Funding acquisition; Validation.

Declaration of interests

☒ The authors declare that they have no known competing financial interests or personal relationships that could have appeared to influence the work reported in this paper.

☐The authors declare the following financial interests/personal relationships which may be considered as potential competing interests:

Highlights

- Cellulose paper-based thermoelectric generators packaged inside Kapton layers are fabricated
- A high output voltage of 84.5 mV and power of 215 nW are obtained at a temperature difference of 50 ºC
- A very simple and economical approach to fabricate paper based eco-friendly thermoelectric devices